https://doi.org/10.5194/cp-2021-49
Preprint. Discussion started: 20 May 2021

Climate of the Past Discussions

Was there a volcanic induced long lasting cooling over the Northern Hemisphere in the mid 6th-7th century?

Evelien van Dijk[1], Johann Jungclaus[2], Stephan Lorenz[2], Claudia Timmreck[2], and Kirstin Krüger[1]

[1]Department of Geosciences, University of Oslo, Oslo, Norway
[2]Max Planck Institute for Meteorology, Hamburg, Germany

Correspondence: Kirstin Krüger (kirstin.krueger@geo.uio.no) and Evelien van Dijk (evelien.van.dijk@geo.uio.no)

Abstract. The climate in the Northern Hemisphere (NH) of the mid-6th century was one of the coldest during the last two millennia. The onset of this cold period is attributed to the volcanic double eruption event in 536 and 540 Common Era (CE) based on multiple paleo-proxies. Recently, there has been a debate about how long lasting and cold this volcanic induced cold period actually was.

To better understand this, we analyze new transient simulations over the Common Era and enhance the representation of mid 6th to 7th century climate by additional ensemble simulations covering 520-680 CE. We use the Max Planck Institute Earth System Model and apply external forcing as recommended in the Paleo Model Intercomparison Project, Phase 4. After the four large eruptions in 536, 540, 574, and 626 CE, a significant surface climate response up to 20 years is simulated. The Northern Hemisphere 2 m air temperature, and precipitation decreases up to 2 K, and 0.2 mm day^{-1}, respectively, and sea ice area increases up to 1.5 $\cdot 10^{12}$ m^2. The global ocean heat content decreases drastically by 1.5$\cdot 10^{23}$ Jm^{-1},which is significant for 30-40 years, and does not totally recover during the entire study period. The surface maps reveal atmospheric circulation changes with a hemispheric dipole pattern and land see contrast in the first two years after the eruptions. Poleward of $\sim$45°N higher sea level pressure and a decrease in hydrological variables occur, accompanied by a land see contrast, with decreased values over land and an increase in values over the ocean, which is especially pronounced for evaporation during boreal summer. During boreal winter, a positive North Atlantic Oscillation develops in the first year after (three out of the four) large eruptions. Analysing underlying mechanisms in the North Atlantic reveals that complex interaction between sea-ice expansion, changes in barotropic streamfunction and meridional overturning circulation leads to a reduction in the ocean heat transport, which then further enhances sea ice expansion impacting NH surface climate up to 20 years.

Temperature records reconstructed from tree-rings in the NH agree well with the model simulations and show a similar $\sim$ 20 year cooling after the eruptions. A century of surface cooling starting in the mid-6th century, as shown from local tree-ring records from the Alps and Altai, does not occur in our volcanic climate model simulations, nor in the NH tree-ring compilation.

1 Introduction

Large volcanic eruptions are the major driver of natural climate variability in the pre-industrial era of the last millennium (Hegerl et al., 2006; Schurer et al., 2014). Previous modeling studies show the Little Ice Age (LIA) being triggered by volcanic

https://doi.org/10.5194/cp-2021-49
Preprint. Discussion started: 20 May 2021


Climate of the Past Discussions

eruptions (Schneider et al., 2009; Miller et al., 2012). Several cluster eruptions and double eruptions occurred in the last 2000 years, coinciding with cold periods in Northern Hemisphere (NH) tree-ring records (Briffa et al., 1998; Sigl et al., 2013). One of the coldest decades of the last 2000 years in Europe and the NH is visible in tree-ring records during the mid-sixth century (e.g., Larsen et al., 2008; Büntgen et al., 2011; Sigl et al., 2015; Büntgen et al., 2020). Historic evidence (Stothers, 1984; Rampino et al., 1988) as well as tree-ring data and ice core records (Baillie, 2008; Larsen et al., 2008) point thereupon that this period was initiated by volcanic eruptions, similar to the LIA. Indeed, four large volcanic eruptions occurred in 536, 540, 574, and 626 CE (Sigl et al., 2015), with the 536/540 CE double eruption creating the strongest decadal volcanic forcing in the last 2000 years, and more than a decade of surface cooling (Toohey et al., 2016a). Reconstructed tree-ring temperatures from the Alps and Altai show a century-long cooling event that might have exceeded that of the LIA (Büntgen et al., 2016). Thus, this period was called the Late Antiquity Little Ice Age (LALIA). However, other tree ring locations from NH extratropics only indicate a multi-decadal cooling until ∼570 CE rather than a centennial one (Helama et al., 2017). With the help of climate models we can test if a series of volcanic eruptions may have caused severe long-lasting cooling over the NH and Europe during the mid 6th to 7th century.

Previous model studies have simulated the surface climate response to volcanic eruptions in the last millennium, and found up to a decade of surface cooling due to extremely large eruptions (Timmreck et al., 2009 Schneider et al., 2009; Stenchikov et al., 2009). If consecutive eruptions occur within a few years, sea ice-ocean feedback mechanisms may maintain the surface cooling over longer time scales, from years to decades (Myhre et al., 2013). A series of decadally-paced volcanic eruptions in the mid 13th century is likely to have caused the onset of the LIA (Zhong et al., 2011; Miller et al., 2012). However, not many modeling studies exist investigating volcanic-climate impacts during the first millennium. Toohey et al. (2016a) carried out climate simulations from 536-550 CE, analyzing the effect of the 536/540 CE volcanic double event on the NH surface climate. The volcanic forcing was reconstructed based on the sulfate deposition in ice cores and the aerosol climate model MAECHAM-HAM (see Table 1), which was used as input for the Max Planck Institute Earth System Model (MPI-ESM) climate simulations. They found decreased NH temperature anomalies of maximum 2°C and increased Arctic sea-ice after the volcanic double event lasting the entire simulation period of 15 years. However, their simulated period of 15 years was too short to study multidecadal cooling. In addition, the simulations from Toohey et al. (2016a) were started from a pre-industrial conditions control run, whereas our simulations include the forcing history of the first half-millennium.

Temperature proxies from several sources have been used to reconstruct the past climate, like tree rings, pollen, corals, lake and marine sediments, glacier ice, speleothems and historical documents. These reconstructions are calibrated against observations, and cover the entire common era (Ahmed et al., 2013). However, most reconstruction data sets go back to about 1200 CE, and the further back in time, the fewer proxy records remain, and the more uncertainties they contain (Masson-Delmotte, 2013; Neukom et al., 2019). The main proxy type that remains to reconstruct the temperatures in the Northern Hemisphere (and especially mid-high latitudes) are tree rings (Ahmed et al., 2013), and this is often used to reconstruct the temperature in es-

https://doi.org/10.5194/cp-2021-49
Preprint. Discussion started: 20 May 2021


Climate of the Past Discussions

pecially Europe (Luterbacher et al., 2016). Therefore, in this study we use tree ring records to compare to the model simulations.

The aim of this study is to investigate whether a multidecadal to centennial cooling may have occurred in the mid 6th to 7th century. We performed 160 year long (520-680 CE) MPI-ESM ensemble simulations branched off one Paleoclimate Modeling Intercomparison Project phase 4 (PMIP4) past2k simulation (Jungclaus et al., 2017). We focus in particular on the NH and European climate in comparison with available temperature proxy reconstructions. In contrast to the study of Toohey et al. (2016a), the short term (years), as well as the long term (decadal to centennial) effects of the 536/540 CE volcanic double event plus the other eruptions during 520-680 CE on the coupled climate system are analyzed. In addition to the surface climate and sea ice impacts, we also study atmospheric and ocean circulation, hydrology and the ocean-sea ice feedbacks in maintaining the climate signal.

In the following Section 2, the model details, set up and experiments, as well as tree-ring data are described. In Section 3, the model results are presented and discussed. Finally, a summary and conclusion are given in Section 4.

2 Methods

2.1 Model and experiment description

2.1.1 The MPI-ESM model

The MPI-ESM1.2.01p5 taken for this study is the low-resolution (LR) version used for the Coupled Model Intercomparison Project phase 6 (CMIP6) and the PMIP4. The atmosphere component (ECHAM6.3, Stevens et al., 2013) has a horizontal resolution of 1.9°x 1.9°and 47 vertical layers (T63L47) up to 0.01 hPa or 80km altitude. The ocean component (MPIOM 1.6 GR1.5/L40, Jungclaus et al., 2013) features a conformal mapping grid with a nominal resolution of 1.5°. The grid poles are placed over Greenland and Antarctica and the actual horizontal resolution ranges from 22 km near Greenland to roughly 200 km in the Pacific Ocean. The vertical grid is represented on 40 unevenly spaced z-levels, with 20 levels in the upper 700 m. A complete description of MPI-ESM1.2 in its CMIP6 configurations, including parameter and tuning choices, is given by Mauritsen et al. (2019).

2.1.2 The PMIP4 - past2k simulations

For its fourth phase, PMIP has selected four experiments as contribution to CMIP6 (Kageyama et al., 2017). In addition to time-slice experiments, the transient simulation over the last millennium “past1000” was chosen as a core experiment. The “past1000” experimental protocol (Jungclaus et al., 2017) describes several extensions to the standard last millennium simulation and includes the tier-3-category “past2k” experiment that covers the entire CE. The aim of the ”past2k” experiment is to extend the scope of the PMIP transient simulations further back into the past and to encourage model-data comparison studies taking full advantage of the past global changes (PAGES) “PAST2K” data base (Martrat et al., 2019). The MPI-ESM

https://doi.org/10.5194/cp-2021-49
Preprint. Discussion started: 20 May 2021


Climate of the Past Discussions

experiments described here are, to our knowledge, the first past2k runs that are fully compliant with the CMIP6 and PMIP4 protocols. The two simulations started from different dates taken from the end of a 1200-year long "spin-down" simulation under constant 1 CE boundary conditions, which was initialized from the MPI-ESM-LR piControl simulation for CMIP6. Only one of these simulations included all the output options necessary to produce CMOR-compliant output (Eyring et al., 2016) for publication on the Earth System Grid Federation (ESGF). This past2k run is referred to as past2k "run 1" from here on, and the other past2k run is referred to as past2k "run 0".

2.1.3 The 520-680 CE simulations

For this study, we ran ten ensemble members for 160 years from 520-680 CE. The simulations are branched off one of the two past2k runs (run 0) in the year 521 by perturbing the climate. For each ensemble member the atmospheric diffusivity was changed by $1 \cdot 10^{-5}$ to simulate slightly different climate states by the year 536 CE, the year of the first large volcanic eruption. The simulations were run with the new volcanic forcing for PMIP4, as well as best estimate conditions for the 6th-7th century (see external forcing section). A common paleo-model set-up is to use 1850 pre-industrial conditions, due to model simulation limitations. For the ensemble mean results (n=12), we included ten ensemble members from the 520-680 CE and two ensemble members from the PMIP4 past2k simulations. The anomalies were calculated by subtracting the mean of 0-1850 CE from the past2k "run 0" from the mean of the volcanic ensemble. The significance was calculated from the 1200 year control run by taking the 2 to 20 year means of the 1200 years, and then taking 4 random time steps from that time series for the 4 large eruptions. This was done 1000 times for each variable, and the standard deviation was then calculated from those new random time series. 1 time or 2 times the standard deviation (1 and 2σ) were then used to calculate the significance.

2.1.4 External forcing

The external forcing for the MPI-ESM simulations follows the protocol by Jungclaus et al. (2017) using the respective default choices for the past1000 experiment. Except for land-use/land-cover change data, all external forcing agents described in Jungclaus et al. (2017), see below, are available for the entire CE. Total solar irradiance and spectral solar irradiance are derived from cosmogenic radio isotopes through a chain of physics-based models (Vieira et al., 2011; Usoskin et al., 2014), and we chose here the 14C-based SATIRE-M version (see Section 3.1). The effect of solar-derived ozone changes is parameterized by a simple scaling scheme. Greenhouse gases (CO_2, CH_4, N_2O) follow the recommendations for CMIP6 (Meinshausen et al., 2016), and the orbital parameters are calculated internally in ECHAM6's calendar routine. The CMIP6 land-use and anthropogenic land-cover changes have been reconstructed for the period 850 to 2014 CE (Jungclaus et al., 2017; Hurtt et al., 2020). The data set is based on modern estimates of division into several agricultural uses and urban areas coming from the Historical Land Use Data Set for the Holocene (HYDE3.2, Klein Goldewijk, 2016). Considering several options (e.g. linear ramp-up) we decided to simply let the land-cover data be constant for the first 850 years of the past2k runs.

https://doi.org/10.5194/cp-2021-49
Preprint. Discussion started: 20 May 2021

Climate of the Past Discussions
Open Access
EGU

120 **Volcanic forcing**

The volcanic forcing used for the runs is described by Jungclaus et al. (2017) with details on the eVolv2k data set being described by Toohey and Sigl (2017). eVolv2k is used in combination with the Easy Volcanic Aerosol module (EVA), as described by Toohey et al. (2016b). The eVolv2k includes estimates of stratospheric sulfur injections (VSSI) and the locations of the eruptions (latitudes) based on ice core data from Antarctica and Greenland. A calibration factor is used to convert the ice
125 core deposition value to stratospheric sulfur loading (Gao et al., 2007). The details of the eruptions occurring in the period of the ensemble runs are given in Fig. 1. Each eruption gives an abrupt increase in aerosol optical depth (AOD), and the differences between them are distinct. In this study, we focus on the four largest eruptions out of the 14 in the study period, where 536 CE and 626 CE are NH extra-tropical eruptions and 540 CE and 574 CE eruptions are tropical eruptions (Table 1). For the NH extra-tropical eruptions, the aerosols are mainly contained within the NH hemisphere, whereas for the tropical eruptions
130 the AOD spreads out over both hemispheres. Figure 1b shows the accumulated AOD per latitude for 15 year intervals, where 535-550 CE stands out as the period with the strongest forcing of the 160-year simulation period.

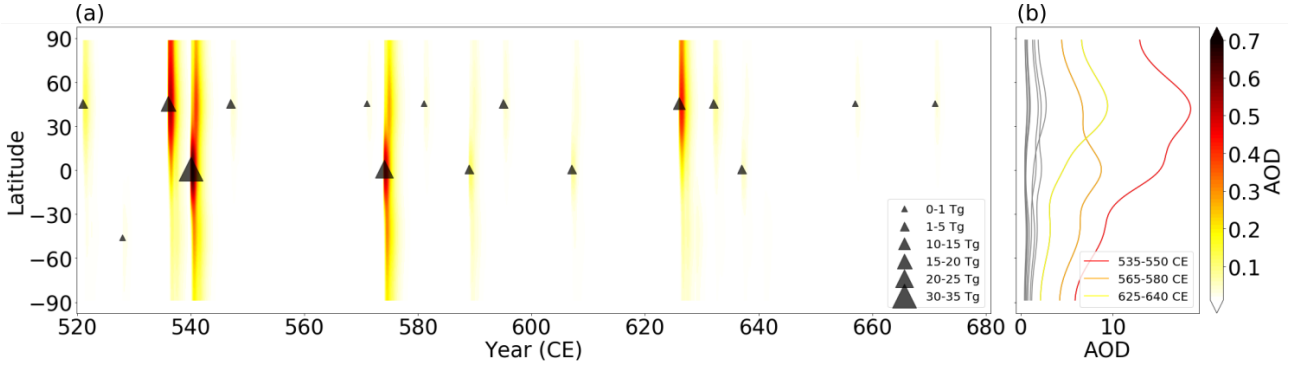

Figure 1. a) Global zonal mean volcanic forcing (Aerosol Optical Depth, AOD) for the study period (520-680 CE) and b) zonal mean accumulated AOD (520-680 CE) in 15 year bins. The three 15 year periods with the highest volcanic forcing are highlighted in color and labeled. The triangles highlight the locations and different strength in terms of stratospheric sulfur injection of all volcanic eruptions as specified in the legend.

2.2 Tree-ring data

For the model-tree-ring comparison, different tree-ring data sets (Stoffel et al., 2015; Büntgen et al., 2016) were used (Table 2). The first four sites combined are the "NH land" compilation by Stoffel et al. (2015) (Figure 5a; this study). The data sets
135 contain a mix of tree ring width (TRW) and maximum latewood density (MXD). TRW has biological memory and gives a lagged and smoothed response to volcanic eruptions. In contrast, MXD is based on cell density, which represents the volcanic climate response well. MXD gives a better representation of surface temperature anomalies (Anchukaitis et al., 2012; Esper et al., 2015; Zhu et al., 2020; Ludescher et al., 2020) and is therefore the preferred target for our model comparison if available.

https://doi.org/10.5194/cp-2021-49
Preprint. Discussion started: 20 May 2021

Climate of the Past Discussions
Open Access
EGU

Table 1. Volcanic forcing and stratospheric sulfur injection for eruptions used in this study (based on eVolv2k; Toohey and Sigl, 2017). Details for the Toohey et al. (2016a) 536 and 540 CE reconstruction based on MAECHAM-HAM are added. The four, respectively, two largest eruptions are highlighted as bold text.

Eruption year	Eruption month	Eruption latitude	S [Tg]	Max global AOD	Reference
521	Jan	NH extratropical	3.7 Tg	0.07	Toohey and Sigl (2017)
528	Jan	SH extratropical	0.8 Tg	0.01	
536	**Jan**	**NH extratropics**	**18.8**	**0.29**	
540	**Jan**	**Tropics**	**31.8**	**0.38**	
547	Jan	NH extratropical	1.1 Tg	0.02	
571	Jan	NH extratropical	0.7 Tg	0.01	
574	**Jan**	**Tropics**	**24.1**	**0.31**	
581	Jan	NH extratropical	0.9 Tg	0.02	
589	Jan	Tropical	4.4 Tg	0.07	
595	Jan	NH extratropical	1.1 Tg	0.02	
607	Jan	Tropical extratropical	2.7 Tg	0.04	
626	**Jan**	**NH extratropics**	**13.2**	**0.21**	
632	Jan	NH extratropical	2.1 Tg	0.04	
637	Jan	Tropical	1.7 Tg	0.03	
657	Jan	NH extratropical	0.7 Tg	0.01	
671	Jan	NH extratropical	0.8 Tg	0.01	
536	**March**	**42°N**	**15**	**0.9**	Toohey et al. (2016a)
540	**Jan**	**15°N**	**25**	**0.9**	

https://doi.org/10.5194/cp-2021-49
Preprint. Discussion started: 20 May 2021


Climate of the Past Discussions

However, as MXD data is sparse during the first millennium, the tree ring proxies consist mainly of TRW data. Only the data from Northern Scandinavia (Esper et al., 2012b, a) consists of MXD. The tree-ring data are given as temperature anomalies with respect to 1961-1990 CE. To account for the different reference periods between the model and tree-ring data, we normalize the data by subtracting the 521-680 CE mean for each data set. The tree-ring sites are displayed in Fig. A1. For the model-tree-ring comparison a land mask was applied to the model 2m air temperature analyzing the NH extratropics between 40°and 75°N. The tree-ring data sets used here capture the boreal summer temperature during June, July and August (JJA) (Stoffel et al., 2015; Büntgen et al., 2016) and were therefore compared to JJA 2m air temperatures from the model.

Table 2. Overview of tree-ring location (see also Fig. A1) and type (MXD: maximum latewood density; TRW: tree ring width) used in this study.

Location name	Coordinates	Type of data	Reference
Nscan	66°-70°N, 19°-29°E	MXD	Esper et al. (2012b, a); Stoffel et al. (2015)
Yamal	66°-68°N, 69°-70°E	TRW	Stoffel et al. (2015)
Taimir	67°-73°N, 88°-105°E	TRW	Stoffel et al. (2015)
Indigirka	70°N, 148°E	TRW	Stoffel et al. (2015)
Alps	46°N, 12.5°E	TRW	Büntgen et al. (2016)
Altai	50°N, 87.5°E	TRW	Büntgen et al. (2016)

3 Results and discussion

3.1 Volcanic response

The four large eruptions in the period 520-680 clearly stand out in the 2m air temperature, precipitation and sea-ice area anomalies, the ocean heat content for the upper 700 m and the global ocean heat transport at 60°N (Figure 2). Variations in the solar forcing are very small compared to the volcanic forcing and can not explain these distinct deviations. Following the 540 CE eruption, maximum deviations are reached during the 520-680 period, with a peak cooling of the NH 2m air temperature of ∼2 K, precipitation decrease of 0.2 mm/day, ocean heat content decrease in the upper 700 m of $1.5 \cdot 10^{23}$ Jm^{-1}, as well as an increase in the Arctic sea-ice area of $1.5 \cdot 10^{12}$ m^2.

The responses in surface climate show a longer recovery than the AOD, indicating that additional processes play a role in cooling the surface climate after volcanic eruptions. The AOD peaks after ∼12 months and is back at background level after 3-4 years (Fig. 2b). The temperature (Fig. 2c) reveals a maximum cooling in the first and second year after the eruption and is decreased for ∼20 years after that, much longer than the direct response of the AOD. The temperature decrease and sea-ice extent increase (Fig. 2e) peak simultaneously, and show a similar long recovery after the eruptions. The precipitation decrease

https://doi.org/10.5194/cp-2021-49
Preprint. Discussion started: 20 May 2021

follows a similar pattern as temperature and sea ice area changes, but with a shorter recovery period. The precipitation anomalies are back to zero after 10-15 years after the eruptions. The global ocean heat content anomaly for the upper 700 m (Fig. 2f) shows a maximum decrease right after the eruptions, which is significant for 30-40 years, and even lasts up to the entire study period. The global ocean heat content is the only variable that reveals a century long anomaly due to the subsequent eruptions. The Atlantic ocean heat transport at 60°N reflects high inter-annual variability, which makes it hard to distinguish any significant volcanic signal. However, after the double volcanic eruption of 536/540 CE there is a significant decrease in northward heat transport visible (Fig. 2g). Towards the end of the simulation period the ensemble shows a larger spread than at the beginning of the simulations, which corresponds to the ocean heat content state being more different between members in the end than at the beginning of the simulations.

Zhong et al. (2011), and Miller et al. (2012) argued that the ocean - sea-ice feedback could play a major role in sustaining a century long cooling after a cluster of four volcanic eruptions in the mid 13th century. In contrast to these studies, we simulate a multi-decadal sea ice response in the mid 6th to 7th century. After the 536/540 CE double event, the ensemble mean of the model simulations does not return to zero sea-ice cover anomalies before 560 CE. This means that the sea-ice is in an anomalous state for more than 20 years after the 536 CE eruption. Following the 574 eruption, the sea-ice area is anomalous for 30 years, and after the 626 eruption the sea-ice area is anomalous for 15 years. More details on the ocean sea-ice feedbacks will be discussed in Section 3.3

https://doi.org/10.5194/cp-2021-49
Preprint. Discussion started: 20 May 2021

Climate of the Past Discussions
Open Access
EGU

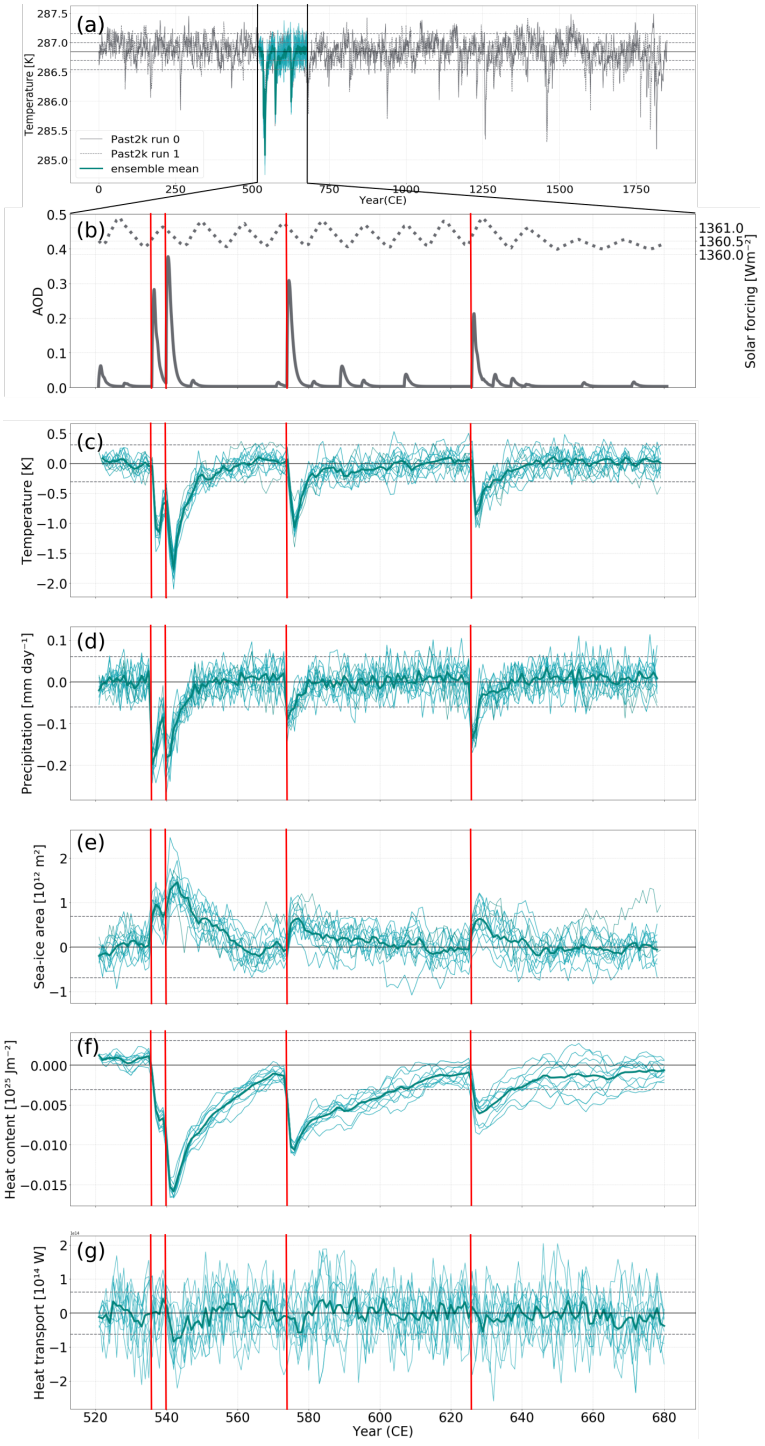

Figure 2. Time series of a) NH 2m air temperature for the two past2k and the MPI-ESM 521-680 CE ensemble runs, b) global AOD volcanic forcing and solar forcing, c) NH 2m air temperature, d) NH total precipitation, e) Arctic sea-ice area, f) global ocean heat content for the upper 700 m, and g) Atlantic ocean heat transport at 60°N. All variables are given as anomalies wrt 0-1850 CE. The timing of the volcanic eruptions in the study period (520-680 CE) are represented by a red line. Ensemble runs are blue and the ensemble mean is the thick blue line. The grey dashed lines indicate the 2σ of the control run.

https://doi.org/10.5194/cp-2021-49
Preprint. Discussion started: 20 May 2021


Climate of the Past Discussions

3.2 Surface climate response

To get more insights into the surface climate response we investigate the spatial patterns of the short-term (2 years) and long-term (20 years) response following the four large eruptions in Fig 3. The maps are shown for boreal winter (DJF) and summer (JJA), where the first two winters after the eruption correspond to year 1 and year 2.

For boreal winter, the short term response shows the most pronounced 2m air cooling over the Hudson Bay, Labrador Sea, Baffin Bay, and surrounding Western, Southern and Eastern Greenland. The sea level pressure (SLP) anomalies reveal increased pressure over high latitudes poleward of 40-50°N, except for Greenland. At the same time, decreased pressure is visible over the Northern Pacific indicating an eastward shift of the Aleutian low and corresponding wind changes. The 10 m wind shows anomalous westerly flow over the North Atlantic north of 50°N, which means increased westerly winds, and anomalous easterly flow, which means reduced westerly winds, south of ∼40 °N. The latitudes north of 40°N show a decrease in precipitation, except for a small area off the west-coast of Norway, whereas south of this latitude it increases. For evaporation there is a land-sea contrast, where south of 40°N there is a decrease over the oceans and an increase over land, and opposite for north of 40°N, with the largest increase in evaporation off the east-coast of Japan. The cloud cover fraction anomaly patterns follow those of precipitation and evaporation closely (not shown).

The boreal summer pattern for 2 years after the eruptions is very similar for 2m air temperature and precipitation. The 2m air temperature is decreased everywhere on the NH, but the cooling is strongest south of ∼45°N over the continents (Fig. 3a), which corresponds to the maximum in AOD (Fig. 1). This separation between south and north of 45°N is also visible in the hydrology, where south of 45°N precipitation and evaporation over land increase while they decrease north of it. In addition, there is a land-sea contrast present for evaporation in summer, where the signal is opposite over the ocean. The SLP in summer is increased over the polar region and over the continents, except for some areas on the western side in North America and Southern Europe. Over the North Atlantic and the North Pacific the SLP shows a decrease at the south side and an increase at the north side of the climatological high pressure systems reflecting an atmospheric circulation separation at around 45°N. The wind anomalies follow the SLP anomaly patterns, with anomalous westerly flow around the decreased low pressure over the Arctic and an anomalous cyclonic pattern around the decreased high pressure systems over the oceans. Wind anomalies above 0.5 m/s only appear over the oceans and coastal regions, not over the continents.

In summary, the SLP, precipitation and evaporation maps show a dipole pattern over the NH with a separation at ∼40°N in winter and ∼45°N in summer, indicating atmospheric circulation changes after two years of the large volcanic eruptions. The wind anomalies show increased surface westerlies north of 60°N, and decreased westerlies south of 50°N over the North Atlantic in NH winter, indicating a positive like North Atlantic Oscillation (NAO) response. To get a better insight in the response after each large eruption, the NAO index (see Figure A2 and corresponding text) is given for the entire study period, as well as an epoch analysis for up to 20 years after the four large eruptions. All except the 536 CE eruption show a positive NAO the first winter after the eruption (year 1) followed by a weak positive or a negative second winter. This leads to a weak positive

https://doi.org/10.5194/cp-2021-49
Preprint. Discussion started: 20 May 2021

Climate of the Past Discussions

NAO response in the 2-year ensemble mean (Figure 3).

210

https://doi.org/10.5194/cp-2021-49
Preprint. Discussion started: 20 May 2021

Climate of the Past Discussions
Open Access
EGU

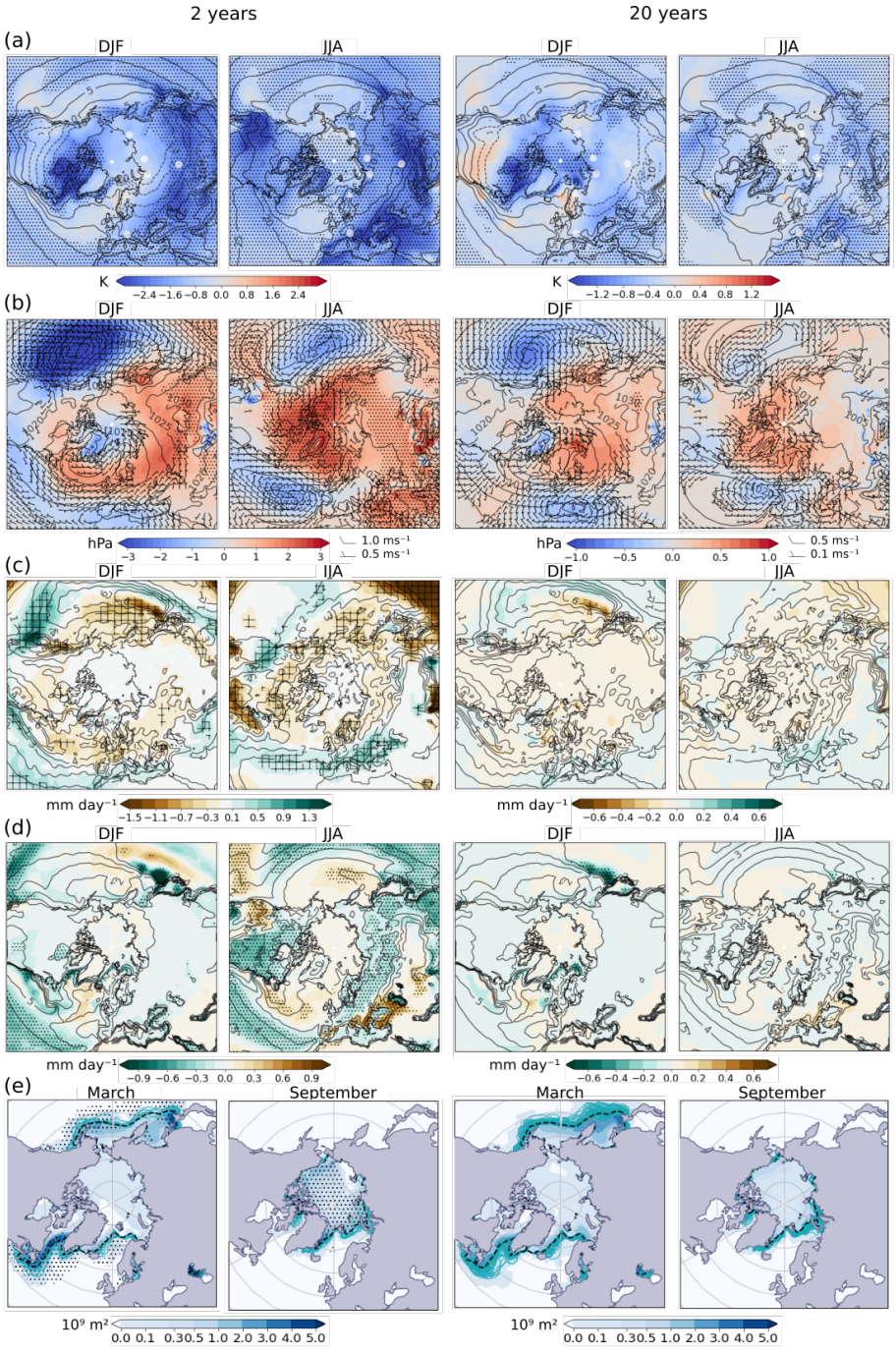

Figure 3. NH maps of boreal winter (DJF) and summer (JJA) (a) 2m air temperature, (b) sea level pressure and 10 m wind, (c) precipitation, (d) evaporation, and (e) March and September sea ice extent and sea-ice area for 2 years and 20 years after the eruptions, poleward from 30°N. The 2 years after the eruption are year 1 and year 2 for DJF, and year 0 and 1 for JJA. All variables are given as anomalies wrt 0-1850 CE, except for sea-ice extent. The 0-1850 CE climatology is given as contours and the tree-ring locations are represented by white dots (TRW) and triangles (MXD) in the 2 m air temperature maps. The 2σ (1σ) standard deviations for 2m air temperature SLP, evaporation (and precipitation) are stippled (hatched). Note the different scales for the 2 year and 20 year maps and that wind anomalies are shown only for 0.5 and 1.0 m/s intervals.

https://doi.org/10.5194/cp-2021-49
Preprint. Discussion started: 20 May 2021


Climate of the Past Discussions

The sea-ice extent as a response to the eruptions (Figure 3e) is given for the maximum and minimum sea ice area months, March and September respectively. For the short term response, the Arctic sea-ice extends southward by at least ∼1-2° from the long term mean (past2k run 0), with the largest changes south of Greenland to south of Newfoundland and in the Pacific during March and in the Barents Sea and Kara Sea during September.

The long term response is shown in the right side of Figure 3. In both winter and summer the patterns are very similar to the 2 year response, only weaker for all variables but the sea-ice extent. For temperature, the main signal that remains is the cooling over the Hudson Bay, the Labrador Sea, east of Greenland towards Svalbard and east of Svalbard in boreal winter. In the same season, the largest SLP anomaly after 20 years is the increased pressure over Scandinavia and Siberia and the decrease over Greenland and the Mediterranean in boreal winter. The sea-ice extent for the long term is extended further south than for the first two years after the eruptions. Especially the Labrador Sea in March and in lesser extend the Barents Sea and Kara Sea in September have an anomalous sea-ice extend, with up to ∼5° and up to ∼3-4° from the 0-1850 mean respectively.

Overall, the NH maps reveal that there is an atmospheric circulation change with a division at mid-latitudes (around 40°N to 45°N) and a land-sea contrast, where the land shows a larger cooling and the opposite signal for precipitation and evaporation as the ocean, lasting up to 20 years after the four large eruptions, where the long term response is only significant for 2m air temperature.

In boreal winter, there is a see-saw pattern visible in the 2 year SLP response with an increased low pressure over Greenland and a decreased low pressure over Northern Europe, corresponding to the seesaw winter temperature pattern between Greenland and Scandinavia, as described by Van Loon and Rogers (1978). The changes in boreal winter reflects a positive Arctic Oscillation pattern, as described by Thompson and Wallace (1998), and typically observed after volcanic eruptions (Robock and Mao, 1992; Stenchikov et al., 2006). After the volcanic eruptions, the climatological high pressure center over the Atlantic in the mid-latitudes gets more confined, which leads to the surface climate patterns with a separation at ∼45°N. From Fig. 3, the 2m air temperature, precipitation and SLP anomalies do not show a clear positive NAO phase for the first two years after the four large eruptions. There is a very small, non-significant warming over western Scandinavia and northwest Siberia in the DJF 2m air temperature anomaly, hinting towards a regional surface winter warming. We have a mean of 12 ensembles, 4 eruptions, and a mix of tropical and extratropical eruptions, which could dampen the signal. When analyzing only the first boreal winter after the eruptions we get a positive NAO response for 3 of the 4 large eruptions (Figure A2). Bittner et al. (2016) analyzed a 100 member ensemble to study the polar vortex and NAO response after volcanic eruptions, and they concluded that for large eruptions (Krakatau/Pinatubo size) at least 15 ensemble members are necessary to get a significant response on the polar vortex.

The summer cooling over the continents can have a serious effect on the vegetation and society, as a few degrees cooling in summer can lead to crop failure and famine in areas that are close to the temperature limit for growing crops. Historic evidence showed the 536/540 CE eruptions delivered crop failure and famine in the Mediterranean (Stothers, 1984; Rampino et al., 1988) and Ireland (Baillie, 1994) and of a collapse of society for Scandinavia (Solberg, 2000; Gräslund and Price, 2012).

https://doi.org/10.5194/cp-2021-49
Preprint. Discussion started: 20 May 2021


Climate of the Past Discussions

The model reconstruction for the 536/540 eruption double event by (Toohey et al., 2016a, see also Table 1) led to the maximum accumulated AOD in the Arctic at around 75°N. The volcanic forcing used for this study is based on eVolv2k (Toohey and Sigl, 2017, see section 2.1.4), which gives the peak AOD at a latitude of 45°N (Fig. A3). According to our spatial pattern of the volcanic forcing we simulate maximum cooling in mid latitudes at around 30-40°N in the Mediterranean, the Himalayas and the Western United States, which are the same areas as Toohey et al 2016a simulated. However, the cooling in our study is stronger. This could be due to the latitudinal difference of the peak volcanic forcing between the two studies.

The increase in precipitation over the Mediterranean in boreal summer in the model simulations in this study are related to the shifting of the inter tropical convergence zone (ITCZ) into the Southern Hemisphere (SH) after the eruptions (not shown here), as well as a weakening of the high and low SLP over the North Atlantic (Figure 3b). After a large volcanic eruption, the ITCZ shifts away from the cooler hemisphere, in this case the NH (Schneider et al., 2009). The southward shift in the ITCZ leads to a weakening of the northern branch of the Hadley cell (Wegmann et al., 2014), which leads to a lower high pressure over southern Europe. This in turn leads to a wetter Mediterranean region, especially in summer (3b-c). Another pattern that becomes evident in the boreal summer months is the land-sea contrast. Over the continents there is a high pressure anomaly, whereas over the oceans there is a low pressure anomaly. This could be due to the radiative effect, where the land responds faster to the cooling effect of the volcanic aerosols. Cold air sinks, which corresponds to a higher pressure.

In boreal summer, the evaporation is increased where the precipitation is also increased, and vice versa. This indicates that the evaporation is more driven by soil moisture availability than by temperature changes. In a colder atmosphere, the air cannot hold as much moisture and becomes saturated sooner, limiting the evaporation (Bala et al., 2008). If the evaporation is driven by the change in temperature one would expect the evaporation to decrease with decreasing 2m air temperature. In this case, there is an increase in precipitation over areas with the strongest cooling, like the Mediterranean, leading to more water being available for evaporation. North of 45°N over the continents, the evaporation anomaly decreases, which corresponds to the decrease in precipitation.

The simulated wettening over the Mediterranean and the drying over Northern Europe in boreal summer is consistent with other studies. Iles and Hegerl (2015) analyzed the hydrological response to 5 large volcanic eruptions between 1901 and 2000 and discovered in their study that the CMIP5 models simulate a wettening over Southern Europe and a drying over Northern Europe, similar to the result in our study. When they compared their model result to observational data, however, the signal appeared to be opposite, with a drying over Southern Europe and a wettening over Northern Europe. They accounted this to the models not capturing the winter NAO well and therefore simulating a different response. Interestingly, our results on hydroclimate and SLP are in accordance with Liu et al. (2020), who used the Community Earth System Model (CESM) to simulated the volcanic effect of the Samalas 1258 CE eruption on the surface climate. In their study, they concluded that the dipole between the drying over Northern Europe and the wettening of the Mediterranean is a result of the weakening of the pressure systems over the North Atlantic and the resulting wind anomalies, as we found in this study for the 521-680 CE ensemble as well.

https://doi.org/10.5194/cp-2021-49
Preprint. Discussion started: 20 May 2021


Climate of the Past Discussions

Hardly any studies have studied the long term response for hydrology after volcanic eruptions. Stevenson et al. (2018) argue that volcanic influences on the multidecadal hydroclimate variability is connected to the Atlantic multidecadal oscillation (AMO) teleconnections, which relates to our results of the SLP anomalies and the corresponding hydroclimate anomaly patterns. However, their focus is on tropical regions and not on the NH mid- to high latitudes.

The SLP anomaly in the long term response over the Barents Sea and Kara Sea corresponds to the sea-ice extent in September. The increase in sea-ice leads to lower air temperature above this area, which causes the air to descend, increasing the SLP. The extended sea-ice in Labrador Sea is important for ocean and sea-ice interactions, which impact the ocean circulation in the North Atlantic (Zhong et al., 2011; Moreno-Chamarro, 2016). We will discuss this in the next section.

3.3 Ocean - sea-ice response

The ocean - sea-ice response can help to maintain the long-lasting cooling in the NH (Zhong et al., 2011). Figure 4 shows the time evolution of the barotropic streamfunction (BTS) and the Atlantic meridional overturning circulation (AMOC) from short term (0-2 years), to mid (3-10 years) and long term (11-30 years) response. The BTS corresponds to the horizontal surface flow, and the AMOC corresponds to the vertical mass streamflow in the ocean.

In the first 5 years after the eruptions, there is a decreased transport visible in the BTS from east of the USA all the way to the British Isles and Iceland of up to 3 Sv (Figure 4a and b). From Fig. 4b and c can be seen that the subpolar gyre (south of Greenland) gets more confined to its center 3-10 years after the eruptions, as there is a strengthening of the flow in the center, whereas the flow at western and eastern sides weakens. At the same time, the transport around 30°- 40°N switches from a weakening to a strengthening flow of more than 3 Sv. After 10 years, the signal in the BTS becomes very small and after 21-30 years, it is almost all back to around 0 anomaly. The only signal that lingers is the weakened eastern part of the subpolar gyre. In the right panels in Fig. 4, a significant decreased streamflow occurs at the surface around 60°N after the first 2 years and 3-5 years after the eruptions. From 3-5 years there is an increase in the streamflow visible at ∼2000 m depth, corresponding to a strengthening of the AMOC. This strengthening peaks at 6-10 years after the eruptions with a significant increase of more than 1 Sv, to decrease again after 10 years. After 20 years the strengthening of the AMOC has disappeared again and the ocean circulation shows hardly any anomalies anymore. Only the decrease in 2-5 years and the 6-10 year increase in AMOC is significant for this volcanic model ensemble, which indicates that the AMOC signal is overwhelmed by internal variability.

A complex interaction between sea-ice expansion, changes in horizontal circulation (BTS) and overturning circulation leads to the reduction in heat transport, which then further enhances sea-ice expansion (Zhong et al., 2011). The sea-ice expansion is most pronounced in the Labrador Sea, which results in a confinement of the subpolar gyre to its center south of Greenland, where it shows a strengthening of ∼3 Sv 2-10 years after the eruptions (4b and c). At the same time, the cyclonic circulation weakens by more than 3 Sv in the eastern basin, which goes along with a reduction of the gyre related heat transports (Jungclaus et al., 2014). In addition, there is a reduction in the Gulf Stream of more than 3 Sv in the first 5 years, followed by a strengthening of the same magnitude in years 6-10. This is consistent with Zanchettin et al. (2012), although they found the strengthening to occur later, 11-15 years after the eruption.

https://doi.org/10.5194/cp-2021-49
Preprint. Discussion started: 20 May 2021


Climate of the Past Discussions

The reduction in streamflow in the Gulf Stream could also be connected to the change in surface wind, as there are anomalous easterlies over the same latitudes in the first two years after the eruptions (Fig. 3). Zanchettin et al. (2012) connected the NAO to the Atlantic ocean circulation through the wind driven subpolar gyre component before.

The expanded sea-ice in the Labrador Sea leads to a deep water formation outside the normal deep water formation areas further south. The sea-ice formation process includes brine rejection, which leads to saltier, and thus more dense surface waters (Zhong et al., 2011), initiating overturning and thus leading to the deep water formation and an increased AMOC from 5 up to 20 years after the eruptions in this study. The increased AMOC then in turn corresponds to the positive anomaly in the subtropics to mid-latitudes of the BTS.

The increased AMOC after the four large volcanic eruptions in this study is consistent with other studies (Otterå et al., 2010; Zanchettin et al., 2012; Swingedouw et al., 2015). Less of a consensus however, exists on the timing of the increase in AMOC, which may be due to the different volcanic forcings, models and initial conditions, from which the experiments were initiated, that were used. Otterå et al. (2010) showed the peak increase 5-10 years after the eruptions in their simulations, whereas Zanchettin et al. (2012) displayed an increased AMOC 11-15 years after volcanic eruptions, and Swingedouw et al. (2015) found the AMOC increase 15-20 years after the eruptions. In our case, the phase of the AMOC in the beginning of the runs is similar for the different ensemble members, which means that the initial conditions are not as widely spread out.

https://doi.org/10.5194/cp-2021-49
Preprint. Discussion started: 20 May 2021

Climate of the Past Discussions
Open Access
EGU

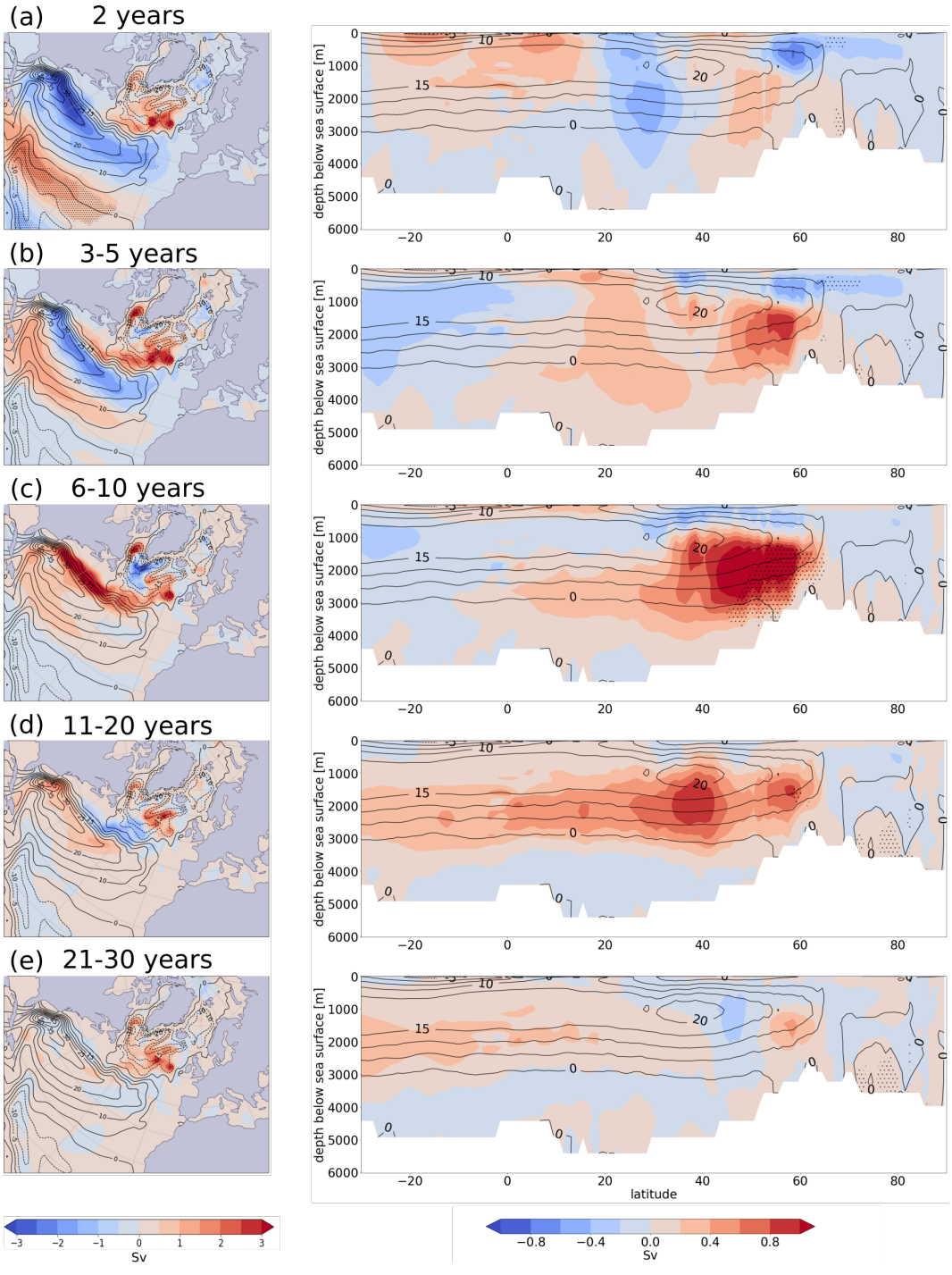

Figure 4. Cross sections of barotropic streamflow (BTS) and Atlantic meridional overturning circulation (AMOC) ensemble mean anomalies for a) 2 years, b) 3-5 years, c) 6-10 years, d) 11-20 years and e) 21-30 years after the four large eruptions. 0-1850 CE climatology in contours. For the BTS anomaly (left panels), negative absolute values indicate anti-clockwise rotation and positive absolute values indicate clockwise rotation. For AMOC (right panels), negative anomalies correspond to a decrease in stream flow, positive anomalies correspond to an increase in stream flow. Anomalies are with respect to the 0-1850 CE background climatology. 2σ significant areas are stippled.

https://doi.org/10.5194/cp-2021-49
Preprint. Discussion started: 20 May 2021


Climate of the Past Discussions

Zanchettin et al. (2012) simulated the ocean-atmosphere response to large volcanic eruptions, and concluded that the sea-ice extent and corresponding deep ocean convection in the North Atlantic was dependent on the initial state of the ensemble member. This led to different model ensembles having different spatial patterns when it comes to deep convection in the North Atlantic. The studies from Zhong et al. (2011) about the onset of the LIA also concluded the response to be depended on the initial state of the North Atlantic, as only 2 out of 4 simulations (one warm and one normal NA state) lead to a cooling long enough to resemble the LIA. Compared to their study, our NA state is relatively warm, but it is hard to compare as a different model and set up were used.

As mentioned before, the differences in timing in ocean circulation responses could be due to the different models used in the different studies. In addition, the volcanic forcing was not the same. The climate simulations are sensitive to both the climate model and the volcanic forcing, so this will give a different climate response. Another reason that the timing is different could be the initial state of the ocean when the volcanic eruptions occur. This is less likely, as 10 ensemble members were run, which showed a range of variability in the same range as the 0-1850 CE variability, where the response to the volcanic eruptions clearly stood out against, see for example Fig. 2. Other studies (Zanchettin et al., 2012; Zhong et al., 2011) used a range of different background conditions in the beginning of their model simulations and found similar results among them. Further research into the role of different forcing sets and different responses between the models is needed to fully understand this discrepancy in response timing between the studies. This could be a task within for example the Volcanic Forcing Model Intercomparison Project (VolMIP, Zanchettin et al., 2016).

3.4 Tree-ring - model comparison

We compare the 2m air temperatures from the model simulations to available temperature reconstructions from tree-ring data. For the model - tree-ring comparison, the model temperature anomalies were taken for grid cells corresponding to the latitude/longitude range for the tree-ring locations. In Fig. 5 the comparison for the NH, the Alps, Altai and Northern Scandinavia are shown.

There is a good agreement between the 520-680 CE simulations and the tree-ring data for the NH and Northern Scandinavia. The temperature anomalies from the model simulations and the 2 sigma variability range fall within the 2 sigma variability of the NH of the model simulations and the timing of the peak cooling after the four large volcanic eruptions agree very well. The peak cooling for the NH model simulations shows a larger cooling than the tree-ring data, with a maximum cooling of 2.0 K for the model and 1.4 K for the tree-ring derived temperatures after the 536 CE eruption.

Figure 5b shows the model - tree-ring comparison for Northern Scandinavia (NScan). Just as for the NH, the variability of the model simulations fall within the variability of the tree-ring temperatures. The peak cooling of the 536 and 540 CE eruptions agree very well both in timing and in signal. This could be because the tree-ring data for Fennoscandinavia consists of MXD data, so there is less time lag and smoothing in the signal (Esper et al., 2015). More deviation is visible for the ensemble mean peak cooling for the 574 and 626 CE eruptions.

https://doi.org/10.5194/cp-2021-49
Preprint. Discussion started: 20 May 2021


Climate of the Past Discussions

The agreement between the tree-ring data and the model simulated temperatures for the Alps and Altai (Fig. 5c and d) is less good than for the NH and Scandinavia, but still remarkable. The lines of the model simulations fall within the variability of the tree-ring temperatures, except for the very end of the time series, and the timing of the 536/540 and 626 CE peak cooling agree well. For the Alps, the recovery time after the 536/540 CE eruptions is longer for the tree-ring temperatures than for the model.

https://doi.org/10.5194/cp-2021-49
Preprint. Discussion started: 20 May 2021

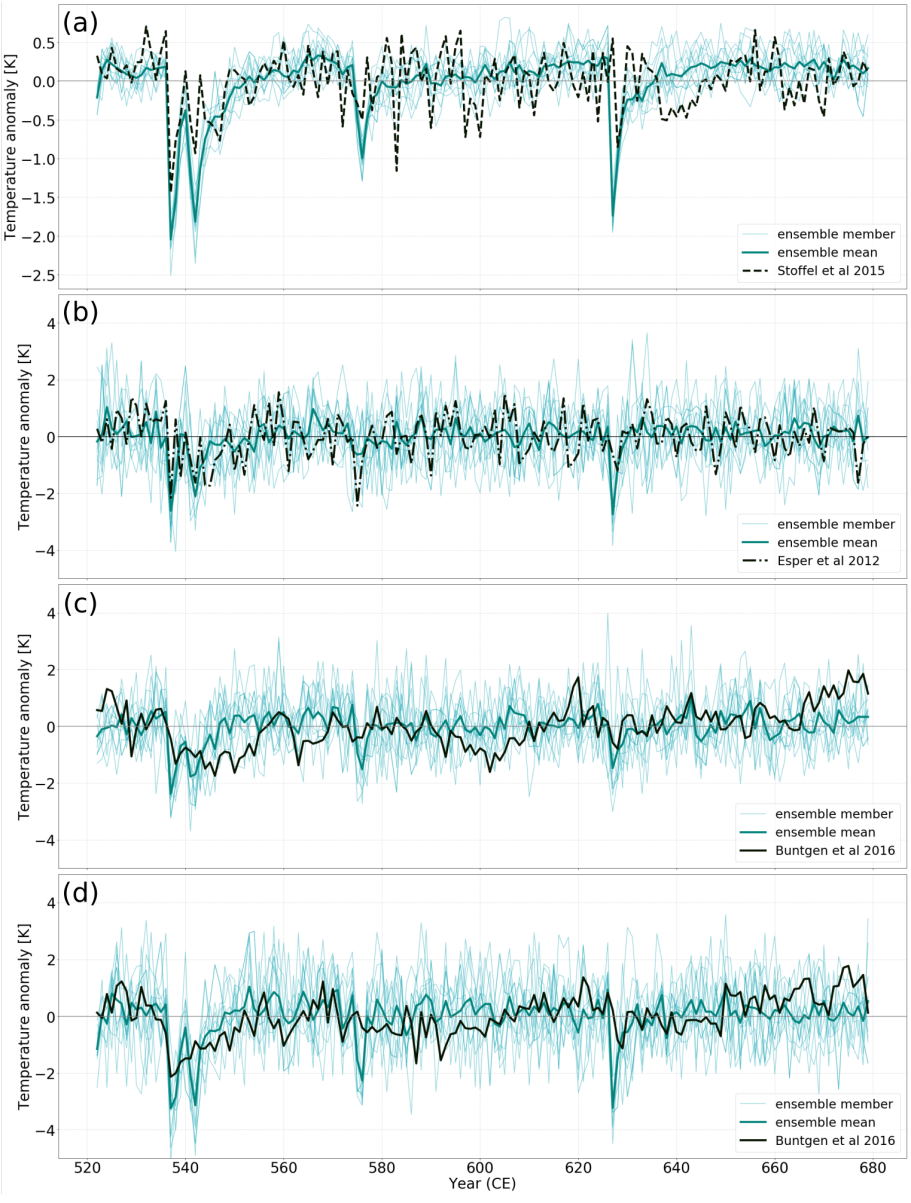

Figure 5. Model–tree-ring comparison for JJA 2m air temperature anomalies from the model with grid cells corresponding to the location of the tree-ring data from a) NH land (40 to 75 °N) (Stoffel et al., 2015); b) Fennoscandinavia (Esper et al., 2012a, b); c) Alps and d) Altai (Büntgen et al., 2016). The mean anomaly of the study period of each data set is subtracted from the anomalies to normalize the data.

The model - tree-ring comparison shows a very good agreement in especially the timing of the 2 m air temperature anomalies. The mismatches that are still present in the NH comparison, like the strength of the peak cooling, could be due to the fact that TRW was used, which gives a lagged and smoothed response (Zhang et al., 2015; Esper et al., 2015; Lücke et al., 2019; Zhu et al., 2020), or because the volcanic forcing in the model is overestimating the cooling in the mid-latitudes. In addition, the

https://doi.org/10.5194/cp-2021-49
Preprint. Discussion started: 20 May 2021


Climate of the Past Discussions

model output is on a 2 by 2° grid, whereas the tree-ring data consists of several single point outputs, that are then averaged. Interestingly, the recovery time of ∼20 year after the peak cooling in the NH tree-ring temperatures is also present in the modeled NH temperature anomalies.

The concept of a LALIA period was raised by Büntgen et al. (2016), based on tree-ring data. There is a good agreement between the tree-ring temperatures and the model temperatures after normalization. This was done with regard to the time series, because the tree-ring temperature anomalies were calculated and provided with respect to the reference period 1961-1990, whereas for the modeled temperature anomalies 0-1850 CE was used as a reference period (see Method Section). The modeled cooling after the volcanic eruptions in 536 and 540 CE after normalization lasts until about 560 CE. The longer cooling after the 536/540 CE eruptions in the tree-ring proxy temperatures of the Alps and Altai could be due to the prescribed volcanic forcing in the model, and that the 547 eruption might have had a stronger impact on NH land than the model simulates.

Previous proxy-based studies (Larsen et al., 2008; Helama et al., 2017) found a cooling up to 570 CE for the NH, where they used a mix of tree-ring, ice-core and documentary records. Only the records from the Alps and Altai show a persistent cooling for a longer period (Büntgen et al., 2016).

In the recent study by Büntgen et al. (2020) an updated tree-ring data set based on 9 tree ring locations for the NH and for the entire past 2000 years was published. This study shows a larger temperature variation than previously recognized for the first millennium, as well as 536 CE marking the beginning of the coldest decade of the last 2000 years. Our findings are also in accordance with the NH compilation of that data set, where there is a cooling until ∼560 CE.

Perhaps the century long lasting cooling may be only apparent in the Alps and Altai tree-ring records, as the cooling is a local feature occurring at high altitude of the mid-latitudes. Our model resolution is too coarse to fully capture the topography of the mountains in the Alps and the Altai, which could explain some model simulations deviation in these areas. Our model ensemble set up with the PMIP4 volcanic forcing reveals up to 25 years of surface cooling over land of the NH extratropics during summer and it also shows the distinct atmospheric circulation response pattern discussed before, for precipitation and evaporation at ∼40°N, separating the Alps and Altai from the other tree-ring locations. The change in hydro-climate corresponds to the soil moisture availability for the trees and thus could have impacted tree ring growth. Future studies are needed to further investigate the multi-model temperature and hydro-climate response on the different regions for the trees, as well as the response to tropical or extratropical eruptions.

4 Summary and Conclusions

In this study, we analyzed new climate model ensemble simulations from 520-680 CE with the MPI-ESM1.2 and eVolv2k PMIP4 volcanic forcing. The aim was to get insights if a series of large volcanic eruptions starting with the onset of the 536/540 CE double eruption event would lead to a century-long lasting cooling (LALIA) in the mid 6th to 7th century in the Northern Hemisphere (NH).

From the model simulations a significant recovery period of up to 20 years is visible after the four large eruptions (536, 540, 574 and 626 CE) in the ensemble mean 2m air temperature, precipitation, and sea-ice area for the NH and in the ocean

https://doi.org/10.5194/cp-2021-49
Preprint. Discussion started: 20 May 2021


Climate of the Past Discussions

heat content for the upper 700 m. The NH 2m air temperature shows a maximum peak cooling of up to 2 K in the year after the 540 CE eruption. NH precipitation is decreased by 0.2 mm day^{-1} after the 536 and 540 CE eruptions and the sea ice area shows a maximum increase of $1.5 \cdot 10^{12}$ m^2 after the double eruption event. For ocean heat content anomaly a decrease of up to $1.5 \cdot 10^{23}$ Jm^{-2} after the double eruption was simulated, which does not fully recover during the entire simulation period. The ocean heat transport has a higher variability compared to the ocean heat content and the signal is not as apparent, but there is a significant decrease of over $2 \cdot 10^{14}$ W after the 536/540 CE eruptions.

The maps for 2m air temperature, sea level pressure (SLP), precipitation and evaporation show a distinct pattern for both boreal summer and winter, where there is a separation of the atmospheric circulation response at ∼40°N in DJF and at ∼45°N in JJA. For the hydrological part, in addition to the atmospheric circulation separation, a land-sea contrast is visible for evaporation in DJF and for JJA the Mediterranean, as well as the west of the US gets wetter, whereas north of 45°N the land areas get dryer. The 2m air temperature map shows a strong cooling over the Hudson Bay, the Labrador Sea and around Greenland in DJF and over the continental mid-latitudes in JJA. SLP is weakened over the Atlantic and the Aleutian low is shifted eastward in DJF, whereas we find increased SLP over the Arctic in JJA. The patterns are generally the same on the long term (20 years after the eruptions), but the signal is much weaker and no longer significant, except for temperature. The sea-ice extent changes are most pronounced in the long term response (20 years after the eruptions) in the Labrador Sea in March and in the Barents Sea and Kara Sea in September, which are important areas for deep water formation and therefore for ocean - sea-ice interactions.

The ocean circulation in the North Atlantic indicates a decrease in the Gulf stream and a confinement of the subpolar gyre in the first 5 years after the eruptions due to the extended sea-ice in the Labrador Sea, which corresponds to a significant decrease in the overturning streamflow. In the following 6 to 10 years, the Gulf Stream is strengthened, whereas the subpolar gyre is still increased in the center and decreased at the western and eastern edges. The sea-ice extents further south for over 20 years after the eruptions, especially in the Labrador sea, shifting the barotropic streamfunction (BTS) to a more confined center and increasing the Atlantic meridional overturning circulation (AMOC), due to brine injection from sea-ice formation, which leads to denser water and increased deepwater formation. Because of this, 3-5 years after the eruptions the AMOC starts to strengthen at 1800 - 2500 m depth, which intensifies and increases to 1000 - 3000 m depth and reaches a significant peak 6-10 years after the eruptions. After 21-30 years the ocean circulation shows no significant anomalies in the AMOC center anymore. The complex interaction between the ocean and sea-ice increase leads to a decrease in ocean heat transport into the Arctic.

The model near surface temperature anomaly during boreal summer agrees well with tree-ring derived temperatures, especially for the NH extratropics and Northern Scandinavia. Northern Scandinavia is the only area where the volcanic induced temperature anomaly agrees so well, probably because of that the tree-ring temperature proxy consists of MXD data. Both the NH tree-ring and model-simulated temperature anomalies show a 20 year cooling after the eruptions before the temperature is back to the zero anomaly line.

In summary, we find in our ensemble-based numerical study of the mid-6th to 7th century that a series of four large and 12 small to medium size volcanic eruptions lead to a significant regional peak cooling of up to 3 K in the NH, an atmospheric circulation change with a hemispheric dipole structure separated at around 40-45°N combined with a land-sea contrast pattern. Analysing underlying mechanisms in the North Atlantic reveals that complex interaction between sea-ice expansion, changes

https://doi.org/10.5194/cp-2021-49
Preprint. Discussion started: 20 May 2021

in the barotropic streamfunction and the Atlantic meridional overturning circulation leads to a reduction in the ocean heat transport, which then further enhances sea ice expansion impacting NH surface climate up to 20 years.

We simulate a significant multi-decadal, but no century-long cooling following the 536, 540, 574, 626 CE and the other eruptions events during 520 CE to 680 CE in good agreement with NH tree-ring temperature reconstructions. Hence, we see no indication of a Late Antiquity Little Ice Age in our model experiment set-up, as discussed in the literature, instead, we obtain a multi-decadal recovery period after the volcanic eruptions where the cold anomaly is sustained by ocean/sea-ice interactions as a result of the volcanic eruptions. Future model studies comparing different models and volcanic forcings with each other are needed to test our results.

Code and data availability. Primary data and scripts used in the analysis and other supplementary information that may be useful in reproducing the author's work are archived and can be obtained by request. Model results will be available under cera-www.dkrz.de. The PMIP4 past2k runs are part of CMIP6 which are available from the ESGF. Tree-ring proxy data can be obtained from NOAA/World Data Service for Paleoclimatology archive https://www.ncdc.noaa.gov/paleo-search.

Author contributions. KK, CT and EvD conceived the original idea. EvD, CT, JJ and SL planned the model simulations. SL and JJ designed the model and the computational framework. EvD carried out the model runs, processed the data, performed the analysis, and designed the figures. KK, CT, JJ contributed to the interpretation of the results. KK supervised the project. All authors discussed the results and helped writing the manuscript.

Competing interests. The authors declare they have no competing interest.

Acknowledgements. This work is funded by the NFR/UiO Toppforsk project "VIKINGS" with the grant number 275191. Computations, analysis and model data storage were mainly performed on the computer of the Deutsches Klima Rechenzentrum (DKRZ), and partly on Sigma2 the National Infrastructure for High Performance Computing and Data Storage in Norway. CT acknowledges support to this research by the Deutsche Forschungsgemeinschaft Research Unit VolImpact (FOR2820,398006378) within the project VolClim (TI 344/2-1). Thanks to Ulf Büntgen and Matthew Toohey for discussions on the results, and to Davide Zanchettin for his help with the significance calculations. Thanks to MPI for Meteorology Hamburg to make a guest exchange possible, which led to the idea for new model experiments of this paper.

https://doi.org/10.5194/cp-2021-49
Preprint. Discussion started: 20 May 2021

Climate of the Past Discussions

References

Ahmed, M., Anchukaitis, K. J., Asrat, A., Borgaonkar, H. P., Braida, M., Buckley, B. M., Büntgen, U., Chase, B. M., Christie, D. A., Cook, E. R., et al.: Continental-scale temperature variability during the past two millennia, Nature geoscience, 6, 339–346, 2013.

Anchukaitis, K. J., Breitenmoser, P., Briffa, K. R., Buchwal, A., Büntgen, U., Cook, E. R., D'arrigo, R. D., Esper, J., Evans, M. N., Frank, D., et al.: Tree rings and volcanic cooling, Nature Geoscience, 5, 836–837, 2012.

Baillie, M. G.: Dendrochronology raises questions about the nature of the AD 536 dust-veil event, The Holocene, 4, 212–217, 1994.

Baillie, M. G.: Proposed re-dating of the European ice core chronology by seven years prior to the 7th century AD, Geophysical Research Letters, 35, 2008.

Bala, G., Duffy, P., and Taylor, K.: Impact of geoengineering schemes on the global hydrological cycle, Proceedings of the National Academy of Sciences, 105, 7664–7669, 2008.

Bittner, M., Schmidt, H., Timmreck, C., and Sienz, F.: Using a large ensemble of simulations to assess the Northern Hemisphere stratospheric dynamical response to tropical volcanic eruptions and its uncertainty, Geophysical Research Letters, 43, 9324–9332, 2016.

Briffa, K. R., Jones, P. D., Schweingruber, F. H., and Osborn, T. J.: Influence of volcanic eruptions on Northern Hemisphere summer temperature over the past 600 years, Nature, 393, 450–455, 1998.

Büntgen, U., Tegel, W., Nicolussi, K., McCormick, M., Frank, D., Trouet, V., Kaplan, J. O., Herzig, F., Heussner, K.-U., Wanner, H., et al.: 2500 years of European climate variability and human susceptibility, Science, 331, 578–582, 2011.

Büntgen, U., Myglan, V. S., Ljungqvist, F. C., McCormick, M., Di Cosmo, N., Sigl, M., Jungclaus, J., Wagner, S., Krusic, P. J., Esper, J., et al.: Cooling and societal change during the Late Antique Little Ice Age from 536 to around 660 AD, Nature Geoscience, 9, 231, 2016.

Büntgen, U., Arseneault, D., Boucher, É., Churakova, O. V., Gennaretti, F., Crivellaro, A., Hughes, M. K., Kirdyanov, A. V., Klippel, L., Krusic, P. J., et al.: Prominent role of volcanism in Common Era climate variability and human history, Dendrochronologia, 64, 125 757, 2020.

Esper, J., Büntgen, U., Timonen, M., and Frank, D. C.: Variability and extremes of northern Scandinavian summer temperatures over the past two millennia, Global and Planetary Change, 88, 1–9, 2012a.

Esper, J., Frank, D. C., Timonen, M., Zorita, E., Wilson, R. J., Luterbacher, J., Holzkämper, S., Fischer, N., Wagner, S., Nievergelt, D., et al.: Orbital forcing of tree-ring data, Nature Climate Change, 2, 862–866, 2012b.

Esper, J., Schneider, L., Smerdon, J. E., Schöne, B. R., and Büntgen, U.: Signals and memory in tree-ring width and density data, Dendrochronologia, 35, 62–70, 2015.

Eyring, V., Bony, S., Meehl, G. A., Senior, C. A., Stevens, B., Stouffer, R. J., and Taylor, K. E.: Overview of the Coupled Model Intercomparison Project Phase 6 (CMIP6) experimental design and organization, Geoscientific Model Development, 9, 1937–1958, 2016.

Gao, C., Oman, L., Robock, A., and Stenchikov, G. L.: Atmospheric volcanic loading derived from bipolar ice cores: Accounting for the spatial distribution of volcanic deposition, Journal of Geophysical Research: Atmospheres, 112, 2007.

Gräslund, B. and Price, N.: Twilight of the gods? The'dust veil event'of AD 536 in critical perspective., Antiquity, 86, 2012.

Hegerl, G. C., Crowley, T. J., Hyde, W. T., and Frame, D. J.: Climate sensitivity constrained by temperature reconstructions over the past seven centuries, Nature, 440, 1029–1032, 2006.

Helama, S., Jones, P. D., and Briffa, K. R.: Limited late antique cooling, Nature Geoscience, 10, 242–243, 2017.

Hurrell, J. W.: Decadal trends in the North Atlantic Oscillation: regional temperatures and precipitation, Science, 269, 676–679, 1995.

https://doi.org/10.5194/cp-2021-49
Preprint. Discussion started: 20 May 2021

Hurtt, G. C., Chini, L., Sahajpal, R., Frolking, S., Bodirsky, B. L., Calvin, K., Doelman, J. C., Fisk, J., Fujimori, S., Goldewijk, K. K., et al.: Harmonization of global land-use change and management for the period 850–2100 (LUH2) for CMIP6, Geoscientific Model Development Discussions, pp. 1–65, 2020.

Iles, C. E. and Hegerl, G. C.: Systematic change in global patterns of streamflow following volcanic eruptions, Nature geoscience, 8, 838–842, 2015.

Jungclaus, J., Fischer, N., Haak, H., Lohmann, K., Marotzke, J., Matei, D., Mikolajewicz, U., Notz, D., and Von Storch, J.: Characteristics of the ocean simulations in the Max Planck Institute Ocean Model (MPIOM) the ocean component of the MPI-Earth system model, Journal of Advances in Modeling Earth Systems, 5, 422–446, 2013.

Jungclaus, J., Bard, E., Baroni, M., Braconnot, P., Cao, J., Chini, L., Egorova, T., Evans, M., González-Rouco, J. F., Goosse, H., et al.: The PMIP4 contribution to CMIP6–Part 3: The last millennium, scientific objective, and experimental design for the PMIP4 past1000 simulations, 2017.

Jungclaus, J. H., Lohmann, K., and Zanchettin, D.: Enhanced 20th century heat transfer to the Arctic simulated in context of climate variations over last millennium, Climate of the Past, 10, 2201–2213, 2014.

Kageyama, M., Albani, S., Braconnot, P., Harrison, S. P., Hopcroft, P. O., Ivanovic, R. F., Lambert, F., Marti, O., Peltier, W. R., Peterschmitt, J. Y., et al.: The PMIP4 contribution to CMIP6-Part 4: Scientific objectives and experimental design of the PMIP4-CMIP6 Last Glacial Maximum experiments and PMIP4 sensitivity experiments, Geoscientific Model Development, 10, 4035–4055, 2017.

Klein Goldewijk, K.: A historical land use data set for the Holocene; HYDE 3.2, EGUGA, pp. EPSC2016–1574, 2016.

Larsen, L. B., Vinther, B. M., Briffa, K. R., Melvin, T. M., Clausen, H. B., Jones, P. D., Siggaard-Andersen, M.-L., Hammer, C. U., Eronen, M., Grudd, H., et al.: New ice core evidence for a volcanic cause of the AD 536 dust veil, Geophysical Research Letters, 35, 2008.

Liu, B., Liu, J., Ning, L., Sun, W., Yan, M., Zhao, C., Chen, K., and Wang, X.: The Role of Samalas Mega Volcanic Eruption in European Summer Hydroclimate Change, Atmosphere, 11, 1182, 2020.

Lücke, L. J., Hegerl, G. C., Schurer, A. P., and Wilson, R.: Effects of memory biases on variability of temperature reconstructions, Journal of Climate, 32, 8713–8731, 2019.

Ludescher, J., Bunde, A., Büntgen, U., and Schellnhuber, H. J.: Setting the tree-ring record straight, Climate Dynamics, 55, 3017–3024, 2020.

Luterbacher, J., Werner, J. P., Smerdon, J. E., Fernández-Donado, L., González-Rouco, F. J., Barriopedro, D., Ljungqvist, F. C., Büntgen, U., Zorita, E., Wagner, S., et al.: European summer temperatures since Roman times, Environmental research letters, 11, 024 001, 2016.

Martrat, B., Eggleston, S., Abram, N., Bothe, O., Linderholm, H., McGregor, H., Neukom, R., Phipps, S., and St George, S.: The PAGES 2k Network: Understanding the climate of the Common Era (past 2000 years), in: Geophysical Research Abstracts, vol. 21, 2019.

Masson-Delmotte, V.: Coauthors, 2013: Information from paleoclimate archives, Climate Change 2013: The Physical Science Basis, 383, 464, 2013.

Mauritsen, T., Bader, J., Becker, T., Behrens, J., Bittner, M., Brokopf, R., Brovkin, V., Claussen, M., Crueger, T., Esch, M., et al.: Developments in the MPI-M Earth System Model version 1.2 (MPI-ESM1. 2) and Its Response to Increasing CO2, Journal of Advances in Modeling Earth Systems, 11, 998–1038, 2019.

Meinshausen, M., Vogel, E., Nauels, A., Lorbacher, K., Meinshausen, N., Etheridge, D., Fraser, P., Montzka, S., Rayner, P., Trudinger, C., et al.: Historical greenhouse gas concentrations, Geoscientific Model Development Discussions, 2016.

https://doi.org/10.5194/cp-2021-49
Preprint. Discussion started: 20 May 2021

Miller, G. H., Geirsdóttir, Á., Zhong, Y., Larsen, D. J., Otto-Bliesner, B. L., Holland, M. M., Bailey, D. A., Refsnider, K. A., Lehman, S. J., Southon, J. R., et al.: Abrupt onset of the Little Ice Age triggered by volcanism and sustained by sea-ice/ocean feedbacks, Geophysical Research Letters, 39, 2012.

Moreno-Chamarro, E.: Climate and ocean variability during the last millennium in paleo-observations and Earth system model simulations, Ph.D. thesis, Universität Hamburg Hamburg, 2016.

Myhre, G., Shindell, D., Bre´on, F.-M., Collins, W., Fuglestvedt, J., Huang, J., Koch, D., Lamarque, J.-F., Lee, D., Mendoza, B., Nakajima, T., Robock, A., Stephens, G., Takemura, T., and Zhang, H.: Anthropogenic and Natural Radiative Forcing, book section 8, p. 659–740, Cambridge University Press, Cambridge, United Kingdom and New York, NY, USA, https://doi.org/10.1017/CBO9781107415324.018, http://www.climatechange2013.org, 2013.

Neukom, R., Barboza, L. A., Erb, M. P., Shi, F., Emile-Geay, J., Evans, M. N., Franke, J., Kaufman, D. S., Lücke, L., Rehfeld, K., et al.: Consistent multi-decadal variability in global temperature reconstructions and simulations over the Common Era, Nature geoscience, 12, 643, 2019.

Otterå, O. H., Bentsen, M., Drange, H., and Suo, L.: External forcing as a metronome for Atlantic multidecadal variability, Nature Geoscience, 3, 688–694, 2010.

Rampino, M. R., Self, S., and Stothers, R. B.: Volcanic winters, Annual Review of Earth and Planetary Sciences, 16, 73–99, 1988.

Robock, A. and Mao, J.: Winter warming from large volcanic eruptions, Geophysical Research Letters, 19, 2405–2408, 1992.

Schneider, D. P., Ammann, C. M., Otto-Bliesner, B. L., and Kaufman, D. S.: Climate response to large, high-latitude and low-latitude volcanic eruptions in the Community Climate System Model, Journal of Geophysical Research: Atmospheres, 114, 2009.

Schurer, A. P., Tett, S. F., and Hegerl, G. C.: Small influence of solar variability on climate over the past millennium, Nature Geoscience, 7, 104–108, 2014.

Sigl, M., McConnell, J. R., Layman, L., Maselli, O., McGwire, K., Pasteris, D., Dahl-Jensen, D., Steffensen, J. P., Vinther, B., Edwards, R., et al.: A new bipolar ice core record of volcanism from WAIS Divide and NEEM and implications for climate forcing of the last 2000 years, Journal of Geophysical Research: Atmospheres, 118, 1151–1169, 2013.

Sigl, M., Winstrup, M., McConnell, J. R., Welten, K. C., Plunkett, G., Ludlow, F., Büntgen, U., Caffee, M., Chellman, N., Dahl-Jensen, D., et al.: Timing and climate forcing of volcanic eruptions for the past 2,500 years, Nature, 523, 543–549, 2015.

Solberg, B.: Jernalderen i Norge: ca. 500 f. Kr.-1030 e. Kr, Cappelen akademisk forlag, 2000.

Stenchikov, G., Hamilton, K., Stouffer, R. J., Robock, A., Ramaswamy, V., Santer, B., and Graf, H.-F.: Arctic Oscillation response to volcanic eruptions in the IPCC AR4 climate models, Journal of Geophysical Research: Atmospheres, 111, 2006.

Stenchikov, G., Delworth, T. L., Ramaswamy, V., Stouffer, R. J., Wittenberg, A., and Zeng, F.: Volcanic signals in oceans, Journal of Geophysical Research: Atmospheres, 114, 2009.

Stevens, B., Giorgetta, M., Esch, M., Mauritsen, T., Crueger, T., Rast, S., Salzmann, M., Schmidt, H., Bader, J., Block, K., et al.: Atmospheric component of the MPI-M Earth system model: ECHAM6, Journal of Advances in Modeling Earth Systems, 5, 146–172, 2013.

Stevenson, S., Overpeck, J. T., Fasullo, J., Coats, S., Parsons, L., Otto-Bliesner, B., Ault, T., Loope, G., and Cole, J.: Climate variability, volcanic forcing, and last millennium hydroclimate extremes, Journal of Climate, 31, 4309–4327, 2018.

Stoffel, M., Khodri, M., Corona, C., Guillet, S., Poulain, V., Bekki, S., Guiot, J., Luckman, B. H., Oppenheimer, C., Lebas, N., et al.: Estimates of volcanic-induced cooling in the Northern Hemisphere over the past 1,500 years, Nature Geoscience, 8, 784–788, 2015.

Stothers, R. B.: Mystery cloud of AD 536, Nature, 307, 344–345, 1984.

https://doi.org/10.5194/cp-2021-49
Preprint. Discussion started: 20 May 2021

Swingedouw, D., Ortega, P., Mignot, J., Guilyardi, E., Masson-Delmotte, V., Butler, P. G., Khodri, M., and Séférian, R.: Bidecadal North Atlantic ocean circulation variability controlled by timing of volcanic eruptions, Nature communications, 6, 1–12, 2015.

Thompson, D. W. and Wallace, J. M.: The Arctic Oscillation signature in the wintertime geopotential height and temperature fields, Geophysical research letters, 25, 1297–1300, 1998.

Toohey, M. and Sigl, M.: Volcanic stratospheric sulphur injections and aerosol optical depth from 500 BCE to 1900 CE, Earth System Science Data, 9, 809–831, 2017.

Toohey, M., Krüger, K., Sigl, M., Stordal, F., and Svensen, H.: Climatic and societal impacts of a volcanic double event at the dawn of the Middle Ages, Climatic Change, 136, 401–412, 2016a.

Toohey, M., Stevens, B., Schmidt, H., and Timmreck, C.: Easy Volcanic Aerosol (EVA v1. 0): an idealized forcing generator for climate simulations, Geoscientific Model Development, 9, 4049–4070, 2016b.

Trenberth, K. E. and Hoar, T. J.: El Niño and climate change, Geophysical Research Letters, 24, 3057–3060, 1997.

Usoskin, I., Hulot, G., Gallet, Y., Roth, R., Licht, A., Joos, F., Kovaltsov, G., Thébault, E., and Khokhlov, A.: Evidence for distinct modes of solar activity, Astronomy & Astrophysics, 562, L10, 2014.

Van Loon, H. and Rogers, J. C.: The seesaw in winter temperatures between Greenland and northern Europe. Part I: General description, Monthly Weather Review, 106, 296–310, 1978.

Vieira, L. E. A., Solanki, S. K., Krivova, N. A., and Usoskin, I.: Evolution of the solar irradiance during the Holocene, Astronomy & Astrophysics, 531, A6, 2011.

Wegmann, M., Brönnimann, S., Bhend, J., Franke, J., Folini, D., Wild, M., and Luterbacher, J.: Volcanic influence on European summer precipitation through monsoons: possible cause for "Years without Summer", Journal of climate, 27, 3683–3691, 2014.

Zanchettin, D., Timmreck, C., Graf, H.-F., Rubino, A., Lorenz, S., Lohmann, K., Krüger, K., and Jungclaus, J.: Bi-decadal variability excited in the coupled ocean–atmosphere system by strong tropical volcanic eruptions, Climate Dynamics, 39, 419–444, 2012.

Zanchettin, D., Bothe, O., Graf, H. F., Lorenz, S. J., Luterbacher, J., Timmreck, C., and Jungclaus, J. H.: Background conditions influence the decadal climate response to strong volcanic eruptions, Journal of Geophysical Research: Atmospheres, 118, 4090–4106, 2013.

Zanchettin, D., Khodri, M., Timmreck, C., Toohey, M., Schmidt, A., Gerber, E. P., Hegerl, G., Robock, A., Pausata, F. S., Ball, W. T., et al.: The Model Intercomparison Project on the climatic response to Volcanic forcing (VolMIP): experimental design and forcing input data for CMIP6, Geoscientific Model Development, 9, 2701–2719, 2016.

Zhang, H., Yuan, N., Esper, J., Werner, J. P., Xoplaki, E., Büntgen, U., Treydte, K., and Luterbacher, J.: Modified climate with long term memory in tree ring proxies, Environmental Research Letters, 10, 084 020, 2015.

Zhong, Y., Miller, G., Otto-Bliesner, B., Holland, M., Bailey, D., Schneider, D., and Geirsdottir, A.: Centennial-scale climate change from decadally-paced explosive volcanism: a coupled sea ice-ocean mechanism, Climate Dynamics, 37, 2373–2387, 2011.

Zhu, F., Emile-Geay, J., Hakim, G. J., King, J., and Anchukaitis, K. J.: Resolving the differences in the simulated and reconstructed temperature response to volcanism, Geophysical Research Letters, 2020.

https://doi.org/10.5194/cp-2021-49
Preprint. Discussion started: 20 May 2021

Climate of the Past Discussions
Open Access
EGU

Appendix A

Figure A1. Locations of the tree-ring sites used in this study from Stoffel et al. (2015) and Büntgen et al. (2016); circles are TRW and triangles MXD data.

NAO

The climate in the North Atlantic and Europe is often indicated by the state of the North Atlantic Oscillation (NAO). The NAO describes variations of the sea level pressure difference between Iceland and the Azores, leading to wind patterns carrying warm moist air to Northern Europe (positive NAO phase), or dry cold air (negative NAO phase). For this study, we calculated the NAO index using the method from Hurrell (1995). The NAO index is calculated from the difference in sea level pressure anomaly between Reykjavik and Lisbon in December, January and February, divided by the standard deviation of that area from the past2k "run 0" (also DJF). The obtained time series then indicates whether the NAO is in a positive or negative phase, where a positive NAO corresponds to relatively warmer and wetter conditions over Scandinavia, and the negative phase corresponding to the opposite (Hurrell, 1995). See Figure A2 and Table A1.

https://doi.org/10.5194/cp-2021-49
Preprint. Discussion started: 20 May 2021

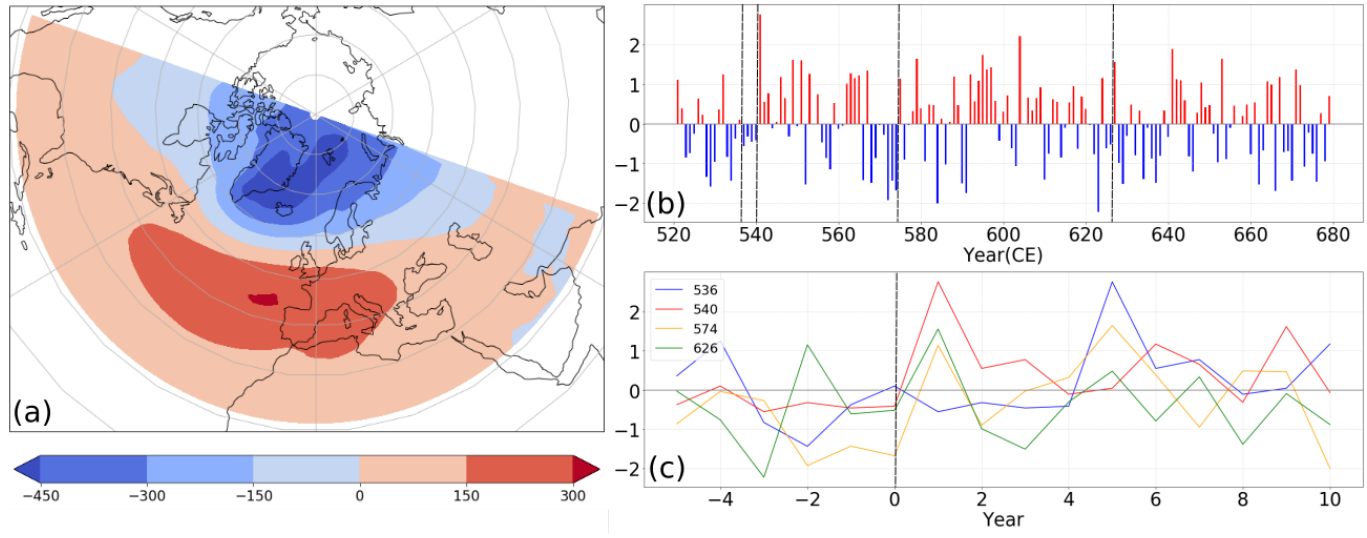

Figure A2. NAO DJF for (a) the climatological NAO signal for 0-1850 CE past2k "run 0", and the response as (b) a time series of the ensemble mean NAO index and (b) an epoch analysis of the NAO index for the four large eruptions during 520 to 680 CE. The eruption years are indicated with a dashed vertical black line. DJF year 0 corresponds to December of the year before the eruption, and January - February the year of the eruption.

https://doi.org/10.5194/cp-2021-49
Preprint. Discussion started: 20 May 2021

Climate of the Past Discussions
Open Access
EGU

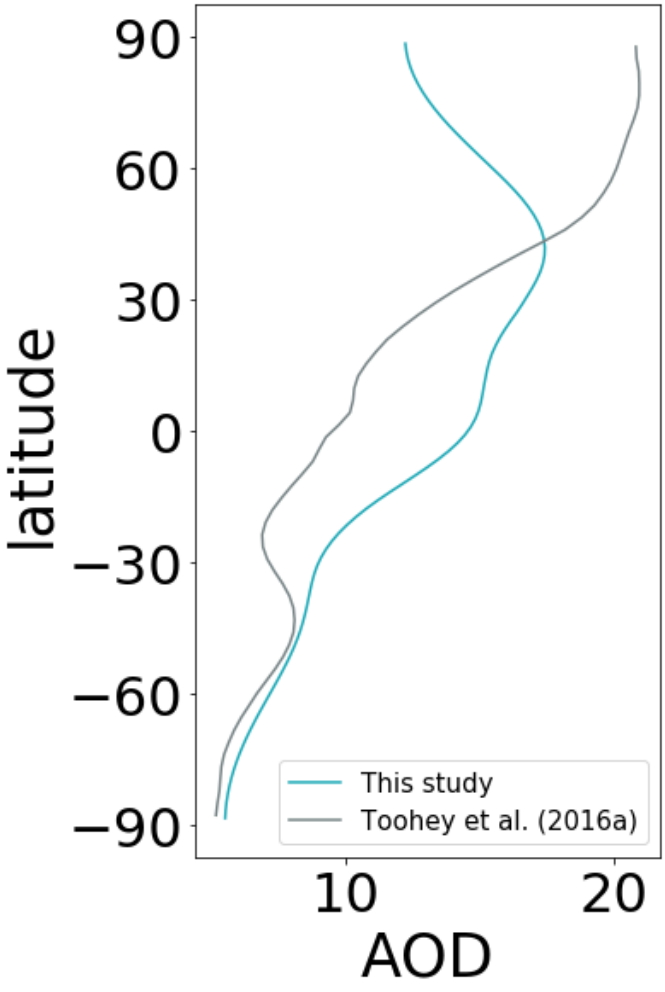

Figure A3. Comparison for accumulated AOD for 536-550 CE for the volcanic forcing from this study (eVolv2k(EVA), Toohey and Sigl, 2017) and from Toohey et al. (2016a) (their Figure 2d, based on MAECHAM-HAM).

Climate indices

Zanchettin et al. (2013) identified the importance of background conditions for ensemble-based numerical studies of large volcanic eruptions as they have an impact on the mechanisms involved in the post-eruption decadal evolution. To determine the background conditions, i.e., the initial climate state of our ensemble members and to address the climate variability during 520 CE to 680 CE several relevant climate indices were calculated.

https://doi.org/10.5194/cp-2021-49
Preprint. Discussion started: 20 May 2021


Climate of the Past Discussions

North Atlantic

Since the focus of this study is on Europe, the initial state of the North Atlantic (NA) ocean and sea ice was calculated. In Table A1, the Atlantic meridional overturning circulation (AMOC), the strength of the barotropic streamfunction (BTS) and the SST for the subpolar gyre are given; Fig. A4 displays the time series of these quantities for the 520-680 CE and past2k runs. The AMOC is defined as the maximum in the mass streamfunction, which occurs between 35°and 45°N and 800 m to 1200 m depth in the MPI-ESM past2k run 0 climatology (0-1850 CE mean). The column integrated BTS can be used as a measure for the strength of the subpolar gyre, which is the horizontal flow south of Greenland with an anticlockwise rotation. The subpolar gyre in the climatology resides between 50°N and 65°N and 20°to 60°W, so we take this area as a measure for the state of the BTS and for the SST. From Table A1 and Figure A4 it becomes clear that the initial ocean and sea ice state before 536 CE covers mean North Atlantic conditions of the past 1850 years. See Figure A4 and Table A1.

ENSO

The El Niño Southern Oscillation (ENSO) index was calculated using the Niño 3.4 index, as described by Trenberth and Hoar (1997). The sea surface temperature (SST) anomaly was calculated for the box 5°S - 5°N and 120°-170°W. If the 5-month running mean exceeds 0.4°C for 6 months or more, the ENSO state is defined as an El Niño (Trenberth and Hoar, 1997). La Niña is defined in the same way, but for -0.4°C instead.

Figure A4 and Table A1 give an overview of the ENSO conditions before the four large volcanic eruptions. The spread in the ensembles cover a wide range of different ENSO states at the beginning of the transient runs.

https://doi.org/10.5194/cp-2021-49
Preprint. Discussion started: 20 May 2021

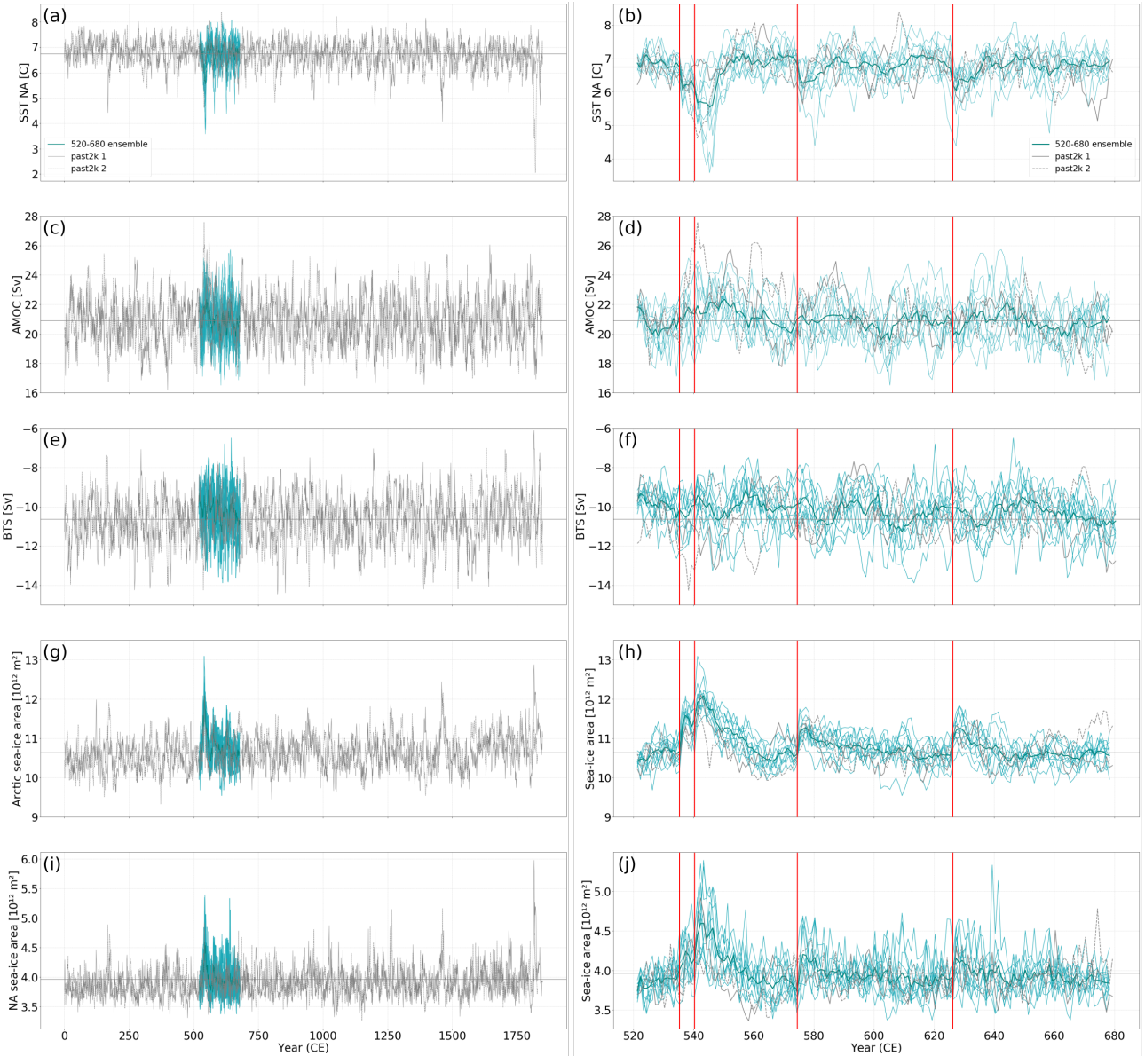

Figure A4. Time series for a/b) NA SST, c/d) AMOC, e/f) BTS, g/h) Arctic sea-ice area and i/j) NA sea-ice for 0-1850 CE (a-e) and 521-680 CE (f-j). The red lines indicate the large volcanic eruptions in the study period, and the straight gray line is the mean of the past2k "run 0".

https://doi.org/10.5194/cp-2021-49
Preprint. Discussion started: 20 May 2021

Climate of the Past Discussions

Table A1. Initial ocean and sea ice conditions. Mean and [range] of all ensemble members for the AMOC, subpolar gyre BTS and SST, NA March sea ice area, and ENSO states (Niño3.4 index) before the four large eruptions. *For all quantities the mean of the previous year of the eruptions are calculated except for the Niño3.4 index, where the 5 month rolling mean (ASOND) of the previous year was taken.

Variable* / Eruption	536 CE (extratropical)	540 CE (tropical)	574 CE (tropical)	626 CE (extratropical)
AMOC [Sv]	20.96 [19.16, 21.77]	21.81 [18.76, 25.82]	20.35 [18.53, 24.25]	20.92 [19.73, 22.31]
Subpolar gyre BTS [Sv]	-10.35 [-8.75, -12.26]	-10.09 [-8.79, -11.29]	-10.16 [-8.71, -11.41]	-10.22 [-8.71, -12.76]
Sub-Polar Gyre SST [°C]	6.69 [6.22, 7.16]	6.28 [5.09, 6.82]	6.97 [6.22, 7.69]	6.65 [4.95, 7.59]
NA March sea-ice area [10^{12} m^2]	3.95 [3.57, 4.48]	4.10 [3.68, 4.84]	3.86 [3.54, 4.23]	3.88 [3.65, 4.65]
Niño3.4 index	2 neutral 5 La Niña 5 El Niño	1 neutral 10 La Niña 1 El Niño	7 neutral 1 La Niña 4 El Niño	6 neutral 4 La Niña 2 El Niño